35th Annual International Conference of the IEEE EMBS
Osaka, Japan, 3 - 7 July, 2013

Microwave technology for localization of traumatic intracranial bleedings—a numerical simulation study

Stefan Candefjord*[1,2,3], Johan Winges[1], Yinan Yu[1,2], Thomas Rylander[1] and Tomas McKelvey[1,2]

Abstract— **Traumatic brain injury (TBI) is a major public health problem worldwide. Intracranial bleedings represents the most serious complication of TBI and need to be surgically evacuated promptly to save lives and mitigate injury. Microwave technology (MWT) is promising as a complement to computed tomography (CT) to be used in road and air ambulances for early detection of intracranial bleedings. In this study, we perform numerical simulations to investigate if a classification algorithm based on singular value decomposition can distinguish between bleedings at different positions adjacent to the skull bone for a similar but simplified problem. The classification accuracy is 94–100 % for all classes, a result that encourages us to pursue our efforts with MWT for more realistic scenarios. This indicates that MWT has potential for localizing a detected bleeding, which would increase the diagnostic value of this technique.**

I. INTRODUCTION

Traumatic brain injury (TBI) is the leading cause of death and severe disability among young people, and frequently occurs in road traffic accidents, sports injuries, etc. [1], [2]. Accidental falls causing TBI among elderly is also a major problem [3]. Intracranial bleedings is the most severe complication of TBI, and need to be detected and treated at an early stage to save the lives of these patients [2]. Computed tomography (CT) is the clinical standard for detecting intracranial bleedings. The main disadvantage with CT is that it is not suitable for portable use. Microwave technology (MWT) could be well suited for field use, as a complement to CT. In previous work we showed by performing laboratory measurements on a bleeding model in a human cranium using a microwave helmet, in addition to 2D numerical simulations of the measurement setup, that MWT is promising for detecting clinically significant bleedings (i.e. large bleedings requiring surgery) and for estimating the size of a bleeding [4], [5]. Imaging the brain in near real-time using MWT is very challenging and currently not feasible [6], [7]. Imaging capability would add to the diagnostic value of MWT. In this study we perform 2D numerical simulations to investigate if there is potential to locate a bleeding by using a classification algorithm trained on a dataset of bleedings at different positions for varying sizes of bleedings in crania of different sizes. As in the previous study [4], [5] we model subdural hematoma, which has very high mortality, 50–85 %, and is the traumatic intracranial bleeding that most commonly requires surgery [1].

This work was supported in part by the Swedish Research Council (dnr 2010-4627) in the project "Model-based Reconstruction and Classification Based on Near-Field Microwave Measurements".

*Asterisk indicates corresponding author.

[1]S. Candefjord, J. Winges, Y. Yu, T. Rylander and T. McKelvey are with the Department of Signals and Systems, Chalmers University of Technology, 412 96, Gothenburg, SWEDEN (stefan.candefjord@chalmers.se; winges@chalmers.se; yinan@chalmers.se; rylander@chalmers.se; tomas.mckelvey@chalmers.se).

[2]S. Candefjord, Y. Yu and T. McKelvey are with MedTech West, Sahlgrenska University Hospital, Blå Stråket 7, 413 45 Gothenburg, SWEDEN.

[3]S. Candefjord is with the SAFER Vehicle and Traffic Safety Centre at Chalmers, Sweden.

II. METHOD

A. Numerical simulations

We exploit numerical simulations for a 2D field problem that resembles a cross section of the microwave helmet measurement setup presented in [4], [5]. The simulations are performed using MATLAB (version R2012a). An example of the 2D geometry is shown in Fig. 1, where the head is surrounded by eight (parallel plate) waveguide antennas with water bags attached to the apertures. (The waveguides have metal walls and the medium in-between the parallel plates has relative permittivity 20 and conductivity 0, chosen to obtain a transmission efficiency similar to the antennas used in the microwave helmet.) The bleedings are modeled as parts of ellipses to mimic the crescent shape of subdural hematomas [2].

We consider the transverse-electric polarization with respect to the z-axis and, thus, the fundamental mode of the waveguides that feed the aperture antennas has zero cut-off frequency. The field problem is solved by means of the finite element method [8] with nodal basis functions of the third order for $H_z(x, y)$. Furthermore, we exploit the first-order boundary condition to model the waveguide ports and the open-region boundary that surrounds the head and the antennas. Given this model of the measurement system, we compute the scattering matrix (including all reflection S_{ii} and transmission coefficients S_{ji} for all combinations of sending antenna i and receiving antenna j) as a function of frequency for the frequency band from 100 MHz to 3 GHz, matching the laboratory measurements [5], for a large number of measurement scenarios that are described below and we estimate the computational relative error to be on the order of percent. The dielectric properties $\epsilon = \epsilon' - j\epsilon''$ of the body tissues and the water (in the water bags) are shown in Fig. 2, where the data for the bone stems from [9] whereas values for gray matter and blood matches the laboratory measurements [5] and water is calculated using a Debye model.

978-1-4577-0216-7/13/$26.00 ©2013 IEEE

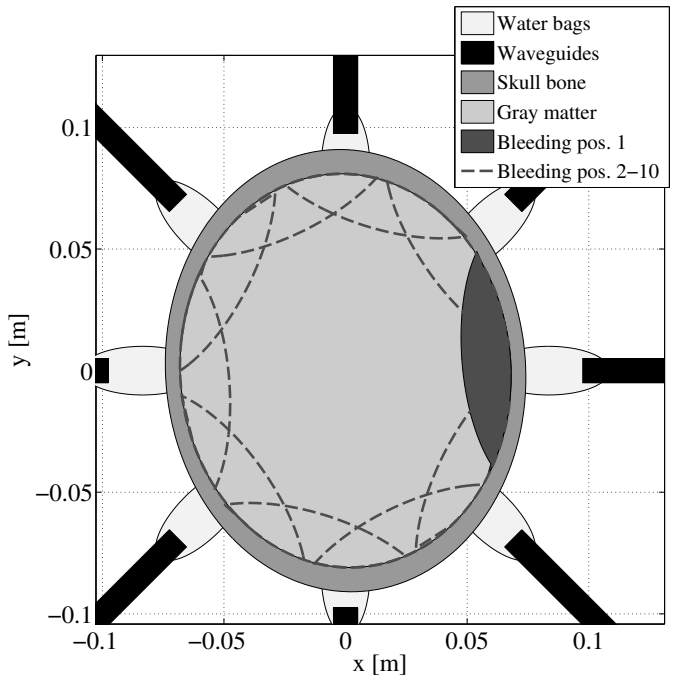

Fig. 1. The 2D geometry that is used in the computational model, here showing bleedings with thickness of 2 cm.

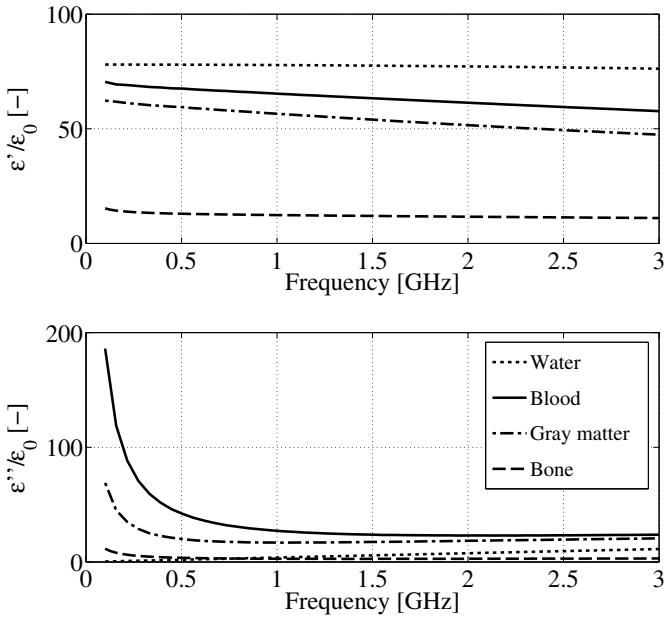

Fig. 2. The dielectric properties $\epsilon = \epsilon' - j\epsilon''$ of the body tissues and the water.

Four parameters are varied in the model in order to incorporate the expected variability for patient measurements:

1) Bleeding positions: We consider ten bleeding positions evenly distributed around the circumference of the inner surface of the skull bone. Fig. 1 shows a bleeding at position 1 by a dark gray area and the other bleeding positions are indicated by means of dashed lines, where the bleeding position index increases in the counterclockwise direction. Since the computational problem is symmetric and simulation times are relatively long, bleedings are first created on the right side of the brain only (positions 9, 10, 1, 2 and 3) and bleedings on the opposite side (positions 4–8) are created by mirroring the geometry and mapping the coefficients S_{ij} to the mirror position (e.g. position $1 \rightarrow 6$, position $2 \rightarrow 7$, etc.).

2) Bleeding sizes: For each bleeding position, the thickness of bleeding takes the values 0.2, 0.5, 1, 2 and 2.5 cm. (A subdural hematoma thicker than 1 cm is considered large and should always be surgically evacuated as soon as possible [2].) Adjacent bleeding positions overlap for bleedings that are thicker than 0.5 cm.

3) Head sizes: The head size is varied by $\pm 6\,\%$ in steps of $2\,\%$ from the base case, which is an ellipse of major axis 18.2 cm and minor axis 14.8 cm equal to the dimensions of the human cranium used in [4], [5], totaling seven head sizes.

4) Helmet positions: The head is rotated randomly by $\pm 6^\circ$ relative to the antenna array. This corresponds to that the antenna that touches the forehead is displaced approximately ± 1 cm in the x-direction.

A dataset with 100 observations per bleeding position is created. Each observation is randomly chosen (without replacement) from a large dataset with approximately even distributions of bleeding sizes, head sizes, and helmet positions. Thus, each class of bleedings, i.e. each position, is composed of many different measurement scenarios, making the classification problem more challenging and mimicking some important aspects of patient measurements.

B. Data preprocessing and analysis

MATLAB (version R2012a) is used for all preprocessing and analysis. Algorithms included in MATLAB are used when possible, other algorithms are written in-house.

1) Preprocessing: For each measurement all channels are combined into one complex vector $\boldsymbol{x}$.

2) Classification algorithm: The bleeding positions represent the different classes. Given C the total number of classes, let $\mathscr{U}_c$ be a subset containing data from class c, where $c \in \{1, \cdots, C\}$. Hence, $\forall\ \boldsymbol{x}_{c,i} \in \mathscr{U}_c$ the signal is modeled as:

$$\boldsymbol{x}_{c,i} = \boldsymbol{U}_c \boldsymbol{\alpha}_c(i) + \boldsymbol{e}_c \tag{1}$$

where $\boldsymbol{U}_c$ is the subspace basis estimated from the measurement matrix $\mathbf{X}_c = \left[\boldsymbol{x}_{c,1}, \cdots, \boldsymbol{x}_{c,N_c}\right]$ by singular value decomposition, with a dimension equal to the number of observations N_c in training data for class c; vector $\boldsymbol{\alpha}_c(i)$ contains the weights of the basis vectors and $\boldsymbol{e}_c$ is additive white noise. Therefore, the classification criterion is to find the smallest distance from the data $\boldsymbol{x}_i$ to the basis $\boldsymbol{U}_c$, for all classes c. For further details about the classification algorithm see [4], [5].

3) Validation: Five-fold cross-validation is used to estimate the classification accuracy.

TABLE I

CONFUSION MATRIX FOR THE CLASSIFICATION RESULT. THE ROWS SHOW THE ACTUAL POSITION OF A BLEEDING AND THE COLUMNS SHOW THE PREDICTED POSITION. THE NUMBER OF OBSERVATIONS CORRECTLY CLASSIFIED (EQUAL TO THE CLASSIFICATION ACCURACY IN PERCENT) FOR EACH CLASS ARE SHOWN IN THE MAIN DIAGONAL (ROW INDEX EQUALS COLUMN INDEX).

	1	2	3	4	5	6	7	8	9	10
1	100	0	0	0	0	0	0	0	0	0
2	0	99	1	0	0	0	0	0	0	0
3	0	1	98	0	0	0	0	1	0	0
4	0	0	0	100	0	0	0	0	0	0
5	0	0	0	0	100	0	0	0	0	0
6	0	0	0	0	2	94	4	0	0	0
7	0	0	0	0	0	1	99	0	0	0
8	0	0	0	0	0	0	0	100	0	0
9	0	0	0	0	0	0	0	0	100	0
10	0	0	0	0	0	0	0	0	3	97

III. RESULTS

Table I and Fig. 3 show the classification results for the different bleeding positions. The classification accuracy was 94–100 % for all classes (Table I). For all classification errors except one a position adjacent to the true one was predicted (Table I). The subspace distance for observations at adjacent positions were in general much smaller than for observations at positions geometrically further away (positions shown in Fig. 1, note that positions 1 and 10 are adjacent) from the current bleeding (Fig. 3).

IV. DISCUSSION

This study shows that MWT has potential for localizing traumatic intracranial bleedings. We simulate a large number of bleedings at ten different positions, of different sizes and in crania of different sizes and demonstrate that the classification algorithm could distinguish the locations with very high accuracy even for a data set with large variability.

A 2D electromagnetic finite element method is employed to achieve a fast and efficient simulation tool that describe the physics for the laboratory measurement setup [4], [5] reasonably well, where the model is rather simple for practical reasons. We consider this to be a suitable approach to simulate patient measurements in the context of a classification algorithm test, since all the input parameters are known and controllable and the fundamental physics and the numerical method is well known and understood. The main limitations of the simulation model are that the anatomy is obviously simplified and that the simulations are performed in 2D, which especially limits the antenna structures that are possible to model. Altogether we can not conclude from the simulation results that it would be possible to localize even small bleedings with high accuracy, but our findings indicate that there is potential for localization of clinically significant bleedings in patients, which would increase the clinical value of MWT.

ACKNOWLEDGMENT

This work has been carried out at SAFER – Vehicle and Traffic Safety Centre at Chalmers, Sweden. The computations were performed on resources at Chalmers Centre for Computational Science and Engineering (C3SE) provided by the Swedish National Infrastructure for Computing (SNIC).

REFERENCES

[1] A. D. Gean and N. J. Fischbein, "Head trauma," *Neuroimaging Clin N Am*, vol. 20, no. 4, pp. 527–556, 2010.

[2] M. Bullock, R. Chesnut, J. Ghajar, D. Gordon, R. Hartl, D. Newell, F. Servadei, B. Walters, and J. Wilberger, "Surgical management of traumatic brain injury," *Neurosurgery*, vol. 58, pp. S2–1–S2–62, 2006.

[3] N. Stocchetti, R. Paterno, G. Citerio, L. Beretta, and A. Colombo, "Traumatic brain injury in an aging population," *Journal of Neurotrauma*, vol. 29, no. 6, pp. 1119–1125, 2012.

[4] S. Candefjord, J. Winges, A. A. Malik, Y. Yu, T. Rylander, T. McKelvey, A. Fhager, and M. Persson, "Microwave technology for detecting traumatic intracranial bleedings—tests on phantom of subdural hematoma and numerical simulations," *IEEE Transactions On Biomedical Engineering*, to be submitted, 2013.

[5] A. A. Malik, "Detecting traumatic intracranial bleedings in a brain phantom using microwave technology," Master's thesis, Chalmers University of Technology, 2012. [Online]. Available: http://publications.lib.chalmers.se/records/fulltext/160183.pdf

[6] S. Y. Semenov and D. R. Corfield, "Microwave tomography for brain imaging: Feasibility assessment for stroke detection," *International Journal of Antennas and Propagation*, p. 254830, 2008.

[7] S. Semenov, "Microwave tomography: review of the progress towards clinical applications." *Philos Transact R Soc A*, vol. 367, no. 1900, pp. 3021–3042, 2009.

[8] J. Jin, *The Finite Element Method in Electromagnetics*, 2nd ed. New York: John Wiley & Sons, 2002.

[9] C. Gabriel, "Compilation of the dielectric properties of body tissues at RF and microwave frequencies, report N.AL/OE-TR-1996-0037," *Occupational and environmental health directorate, Radiofrequency Radiation Division, Brooks Air Force Base, Texas (USA)*, 1996.

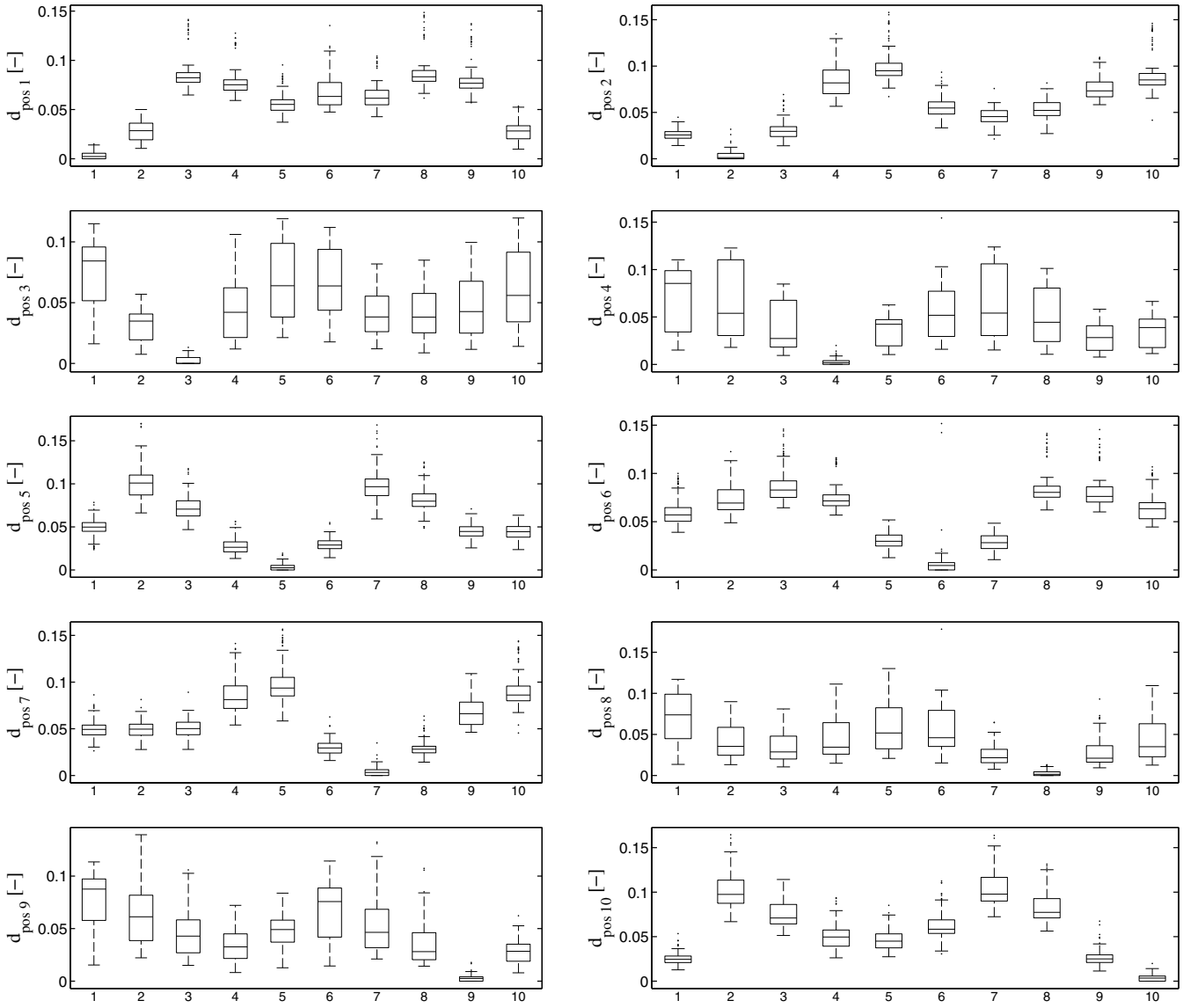

Fig. 3. Box plots showing the distance to each subspace for all classes, i.e. bleeding positions. The line in the middle of the box shows the median, and the bottom and the top of the box show the 25th and 75th percentile, respectively. The whiskers extend to 1.5 times the interquartile range away from the top or bottom of the box, or to the furthest observations from the box. Data points outside the whiskers are plotted individually.